# Hard photons in proton-nucleus collisions

K. Nakayama*
*Institut fur Kernphysik, Kernforschungsanlage Julich, D-5170, Julich, West Germany*

G. F. Bertsch
*Department of Physics and Astronomy and Cyclotron Laboratory, Michigan State University, East Lansing, Michigan 48824*
(Received 14 June 1989)

A calculation of energetic photon production in proton-nucleus reactions at intermediate bombarding energies is performed assuming the first chance nucleon-nucleon collisional mechanism. The elementary nucleon-nucleon bremsstrahlung amplitude is calculated within a meson exchange potential model which includes the one-body as well as the two-body current contributions. The results are in reasonable agreement with the recent data by the Grenoble group at the proton incident energy of $T_{\rm lab}=168$ MeV and indicate that these energetic photons are created in a relatively low-density region in the nucleus ($\sim 40\%$ of the nuclear matter normal density). The present model, however, cannot account for the strong angular dependence observed at $T_{\rm lab}=72$ MeV.

## I. INTRODUCTION

The investigation of energetic products in nuclear reactions is of great importance since these products carry information about nuclear reaction dynamics. Among them, the photon is of particular interest because the weakness of the electromagnetic interaction makes it a clean probe. In fact, in the last few years the observation of hard photons produced in intermediate-energy heavy-ion collisions has led to considerable efforts to understand the underlying dynamics.[1-5]

To test the theoretical models of photon production, it is important to study nucleon-nucleus collisions, since these are much simpler to treat than heavy-ion collisions. Indeed, in Ref. 6, in connection to the nucleon-nucleon ($NN$) bremsstrahlung, we have also investigated nucleon-nucleus bremsstrahlung. However, there we were able to reproduce the data then available only under certain extreme conditions. Very recently, new data on the hard photon production in proton-nucleus collisions became available,[7,8] which show that the earlier data of Ref. 9 is off by a factor of $\sim 3$. Therefore, in the present work we analyze these new data.

## II. NUCLEON-NUCLEUS BREMSSTRAHLUNG

The formalism we use to calculate the nucleon-nucleus bremsstrahlung is the same as in Ref. 6. We express the photon emission probability per unit solid angle and unit photon energy as

$$\frac{d^2P}{d\omega\, d\Omega}=\frac{1}{W_{NN}}\frac{d^2W_{pA\gamma}}{d\omega\, d\Omega}\ , \tag{2.1}$$

where $d^2W_{pA\gamma}/d\omega\, d\Omega$ denotes the nucleon-nucleus bremsstrahlung differential transition rate and $W_{NN}$ the total $NN$ collisional rate irrespective of the bremsstrahlung. We calculate these quantities in the nuclear matter approximation. The photon emission probability should be rather insensitive to certain kind of effects such as the distortion of the wave functions or the strength of the interaction since it is given as a ratio between the two quantities.

The nucleon-nucleus bremsstrahlung transition rate is obtained by folding the elementary $NN$ bremsstrahlung transition rate with the phase-space distribution function of the target nucleus

$$\frac{d^2W_{pA\gamma}(\mathbf{p}_1)}{d\omega\, d\Omega}=\frac{1}{\varepsilon_1}\int_{<k_f}\frac{d^3p_2}{(2\pi)^3\varepsilon_2}2\pi\omega\int\frac{d^3p_1'}{(2\pi)^3\varepsilon_1'}\frac{d^3p_2'}{(2\pi)^3\varepsilon_2'}Q$$
$$\times\left[\frac{1}{4}\sum_{\substack{SM_S\\ S'M_{S'}}}\sum_{\epsilon}\left|\sqrt{\varepsilon_1'\varepsilon_2'\omega}\langle\epsilon,\mathbf{k};\mathbf{p}_1'\mathbf{p}_2'S'M_{S'}|V_{\rm em}|0;\mathbf{p}_1\mathbf{p}_2SM_S\rangle\sqrt{\varepsilon_1\varepsilon_2}\right|^2\right]$$
$$\times\delta^3(\mathbf{p}_1+\mathbf{p}_2-\mathbf{p}_1'-\mathbf{p}_2'-\mathbf{k})\delta(\varepsilon_1+\varepsilon_2-\varepsilon_1'-\varepsilon_2'-\omega)\ . \tag{2.2}$$

In the above equation, the primed (unprimed) quantities refer to the final (initial) two interacting nucleons' energies $\varepsilon_1',\varepsilon_2'$ ($\varepsilon_1,\varepsilon_2$), momenta $\mathbf{p}_1',\mathbf{p}_2'$ ($\mathbf{p}_1,\mathbf{p}_2$), total spin $S'$ ($S$), and its projection $M_{S'}$, ($M_S$). The matrix element in the large parentheses denotes the photon emission amplitude for a photon with polarization $\epsilon$ and momentum $\mathbf{k}$; $\omega$ denotes its

 

energy. The target is characterized only by its Fermi momentum $k_f$. The Pauli blocking operator $Q$ excludes the target Fermi sphere; in the nuclear matter rest frame

$$Q=\theta(p_1'-k_f)\theta(p_2'-k_f) \ . \tag{2.3}$$

Analogously, the total $NN$ collisional rate is given by

$$W_{NN}(\mathbf{p}_1)=\frac{1}{\varepsilon_1}\int_{<k_f}\frac{d^3p_2}{(2\pi)^3\varepsilon_2}\int\frac{d^3p_1'}{(2\pi)^3\varepsilon_1'}\frac{d^3p_2'}{(2\pi)^3\varepsilon_2'}Q\left[\frac{1}{4}\sum_{\substack{SM_S\\S'M_{S'}}}\left|\sqrt{\varepsilon_1'\varepsilon_2'}\langle\mathbf{p}_1'\mathbf{p}_2'M_{S'}|G|\mathbf{p}_1\mathbf{p}_2SM_S\rangle\sqrt{\varepsilon_1\varepsilon_2}\right|^2\right]$$
$$\times(2\pi)^4\delta^3(\mathbf{p}_1+\mathbf{p}_2-\mathbf{p}_1'-\mathbf{p}_2')\delta(\varepsilon_1+\varepsilon_2-\varepsilon_1'-\varepsilon_2') \ , \tag{2.4}$$

where $G$ denotes the $NN$ $G$ matrix associated with the bare $NN$ potential used.

The single-particle energies appearing in Eqs. (2.2) and (2.4) contain not only the kinetic energy but also the potential energy due to the mean field of the target nucleus. We assume the single-particle energies to have the relativistic form[10]

$$\varepsilon(p)=(\mathbf{p}^2+m^{*2})^{1/2} \ , \tag{2.5}$$

where the effective mass $m^*$ is defined as

$$m^*=m+u_s \ . \tag{2.6}$$

Here $u_s$ is the scalar potential; $m$ stands for the nucleon mass. The actual single-particle energy $E(p)$ is related to that of Eq. (2.5) by[10] (in the nuclear matter rest frame)

$$E(p)=\varepsilon(p)+u_0 \ , \tag{2.7}$$

where $u_0$ denotes the timelike component of the vector potential. In principle, both $u_s$ and $u_0$ depend on the momentum $\mathbf{p}$ of the particle. However, here we assume them to be momentum independent, which seems to be a very reasonable approximation.[11]

The bremsstrahlung amplitude in Eq. (2.2) has been calculated within a meson exchange potential model[6] where the strongly interacting particles are treated to all orders in perturbation theory while the coupling to the photon is considered only in first order. The model includes the convection, magnetization, as well as important exchange current contributions, so that the photon emission potential $V_{\rm em}$ is written as a sum of three terms

$$V_{\rm em}=V_{\rm conv}+V_{\rm magn}+V_{\rm exch} \ , \tag{2.8}$$

where $V_{\rm conv}$, $V_{\rm magn}$, and $V_{\rm exch}$ denote the convection, magnetization, and two-body current contributions, respectively. The latter is dominantly the exchange currents.[12] We have previously parametrized the amplitudes in Eq. (2.8) by simple functions of the nucleon and photon energies,[13] and we use that parametrized form in the present calculation. Here we consider contributions only from proton-neutron ($pn$) collisions because they are much more efficient to produce photons than proton-proton ($pp$) collisions. The former processes originate a dipole radiation in lowest order while the latter contribute to the quadrupole radiation. Indeed, the $pp$ bremsstrahlung is roughly a factor of 4 smaller than the corresponding $pn$ bremsstrahlung in the relevant region of photon energy here.[14] In principle, the bremsstrahlung amplitude also contains medium effects (in particular, we should use the $G$ matrix instead of the $T$ matrix); however, we have shown in Ref. 6 that these effects are small and therefore may be neglected. For consistency, the $T$ matrix is used also in Eq. (2.4). A more fundamental problem that arises in medium is related to the photon-nucleon coupling vertex itself. The electromagnetic form factors may (and probably will) change in the nuclear medium from those in the free space.[15] This is as yet an unsolved problem and certainly beyond our scope here. We keep them unchanged from their values in free space.

The cross section is obtained by multiplying the probability rate given by Eq. (2.1) by the cross sectional area of the target

$$\frac{d^2\sigma}{d\omega\,d\Omega}=\pi R^2\frac{d^2P}{d\omega\,d\Omega} \ , \tag{2.9}$$

with $R=1.25A^{1/3}$ fm and $A$ being the mass number of the target nucleus.

We now consider the parameters in the present calculation. They are the Fermi momentum $k_f$, the effective mass $m^*$ (or the scalar potential $u_s$) and the vector potential $u_0$. Note that $u_0$ enters only for the determination of the local momentum of the incident nucleon.

The results will be rather sensitive to the Fermi momentum, so we will estimate it taking nuclear surface effects explicitly into account. We first find the average density at the $NN$ collision point from an eikonal model,

$$\langle\rho\rangle=\frac{\int_0^\infty d^2b\int_{-\infty}^{+\infty}dz\,\rho(b,z)\sigma\rho(b,z)\exp\left[-\int_{-\infty}^{z}dz'\sigma\rho(b,z')\right]}{\int_0^\infty d^2b\int_{-\infty}^{+\infty}dz\,\sigma\rho(b,z)\exp\left[-\int_{-\infty}^{z}dz'\sigma\rho(b,z')\right]} \ . \tag{2.10}$$

Here $\sigma$ is the $NN$ cross section and $\rho$ is the nuclear density. It is assumed to have the form

$$\rho(b,z)=\frac{\rho_0}{1+\exp[(r-R)/a]} , \tag{2.11}$$

with $\rho_0=0.17$ fm$^{-3}$, $a=0.65$, and $r=(b^2+z^2)^{1/2}$.

Given the average density from Eq. (2.10), we find the Fermi momentum from the Thomas-Fermi relation

$$k_f=\left[\frac{3\pi^2\langle\rho\rangle}{2}\right]^{1/3} . \tag{2.12}$$

Next we extract the single-particle energy on the Fermi surface. For a given target nucleus and proton incident energy $T_{\rm lab}$, the maximum photon energy $\omega_{\rm max}$ is

$$\omega_{\rm max}=T_{\rm lab}+S_p , \tag{2.13}$$

where $S_p$ is the proton separation energy in the nucleus with one more proton than the target. Now, within our model, energy conservation yields for the proton energy on the Fermi surface

$$E(k_f)+\Delta E_c=-S_p . \tag{2.14}$$

Here, $\Delta E_c\sim e^2Z/R_c$ stands for the Coulomb energy of the proton. The preceding equation, thus, gives us the proton energy (the nuclear part) $E(p)$ at $p=k_f$. This determines the vector potential $u_0$ in terms of the effective mass $m^*$,

$$u_0=E(k_f)-(k_f^2+m^{*2})^{1/2} . \tag{2.15}$$

We treat $m^*$ as a free parameter to be adjusted to best reproduce the data.

For later convenience we define the mean-field potential energy as

$$U(p)=E(p)-(p^2+m^2)^{1/2} . \tag{2.16}$$

## III. RESULTS

In this section we compare our results with the recent data by the Grenoble group.[7,8]

Figure 1 shows our results for $p+^{159}$Tb at $T_{\rm lab}=168$ MeV and for a photon emission angle of $\theta=90°$ as a function of photon energy and for various value of the effective mass. At this incident energy the $NN$ cross section inside nucleus is about $\sigma=41$ mb.[16] Equations (2.10)–(2.12), then, give for the Fermi momentum the value of $k_f=1.04$ fm$^{-1}$ which corresponds to about 45% of the nuclear matter normal density. Then, the mean-field potential energy at the Fermi surface, extracted from Eq. (2.16), is

$$U(k_f=1.04\ \text{fm}^{-1})=-41.7\ \text{MeV} .$$

This is a quite reasonable value as compared, for example, to those from phenomenological optical potentials.

As can be seen from Fig. 1, the influence of the effective mass is to enhance the cross sections. One of the effective mass dependences arises from the determination of the local momentum of the incident nucleon. As $m^*$ decreases the local momentum increases which means that the effective nucleon energy increases. Now, the $NN$ bremsstrahlung transition rate depends very little on the incident energy,[6] while the total $NN$ collisional rate has a rather strong incident energy dependence and it decreases as the incident energy increases. Since what determines the photon cross section for nucleon-nucleus bremsstrahlung is the ratio between the bremsstrahlung rate and the total collisional rate (the latter is independent on the photon energy), we see that the cross section will be shifted up if the effective mass is decreased. The effective mass has also another effect on the photon cross sections which comes from energy conservation. In the $NN$ center-of-mass (c.m.) frame we have

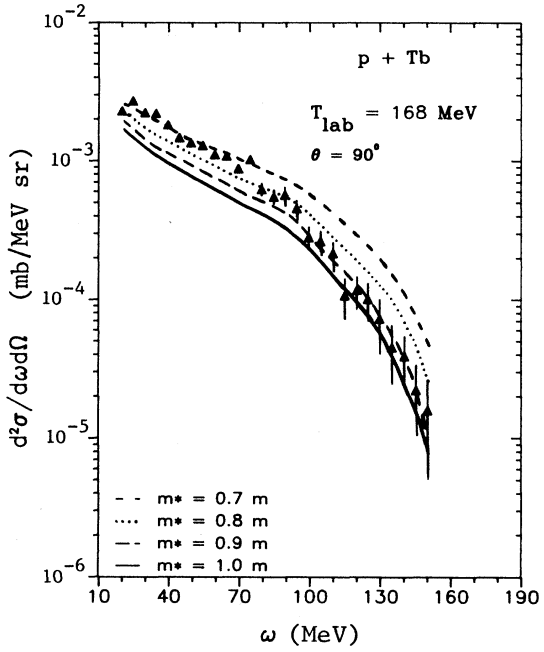


FIG. 1. The bremsstrahlung differential cross section (in the laboratory system) for $p+^{159}$Tb at the incident energy of $T_{\rm lab}=168$ MeV as a function of photon energy and for different choices of the effective mass $m^*$ (in units of nucleon mass $m$). The photon emission angle is $\theta=90°$. The Fermi momentum is fixed to be $k_f=1.04$ fm$^{-1}$. The data are from Ref. 8.

$$2\epsilon(p)=\varepsilon(|\mathbf{p}'+\mathbf{k}/2|)+\varepsilon(|\mathbf{p}'-\mathbf{k}/2|)+\omega_{\rm c.m.} , \tag{3.1}$$

where $\mathbf{p}(\mathbf{p}')$ denotes the initial (final) $NN$ relative momentum and $\omega_{\rm c.m.}$ the photon energy. This gives

$$p'\simeq[p^2-\varepsilon(p)\omega_{\rm c.m.}]^{1/2} . \tag{3.2}$$

From the preceding equation we see that if the effective mass is decreased the available final-state phase space will increase since the single-particle energy $\varepsilon(p)$ as defined in Eq. (2.5) will decrease. It is also easy to see that this effect increases as the photon energy increases. This explains the larger enhancement of the photon cross sections for higher photon energies as $m^*$ decreases in Fig. 1. We observe that the conditions given by Eqs. (2.14)

and (2.15) are always satisfied for different values of $m^*$.

From Fig. 1, we see that the effective mass of $m^* \sim 0.9m$ seems to best reproduce the data in the high photon energy region ($\omega > 75$ MeV). This value of the effective mass also seems reasonable. In the low-energy region, the data prefer a much smaller value of $m^*$, but for such a low density this is probably unrealistic. We will discuss this problem later and take for the moment the value of $m^* = 0.9m$ since we are primarily interested in the high-energy tails.

Once the $m^*$ is fixed, all the parameters are fixed and we can now compare the present predictions with the data. In Fig. 2 the results for the same system as in Fig. 1 are shown for different photon emission angles. As we can see, the agreement is reasonable for high-energy photons. Here, it is worthwhile to mention that, in the laboratory frame, the available phase space for backward emissions is less than for forward emissions. This is easy to see from Eq. (3.2) together with the fact that the photon energy transforms from the laboratory to the $NN$ c.m. system according to

$$\omega_{\text{c.m.}} = \gamma(1 - \beta \cos\theta)\omega \ , \tag{3.3}$$

where $\omega$ and $\theta$ denote the photon energy and emission angle in the laboratory frame and $\beta$ and $\gamma$ are the usual Lorentz frame transformation parameters. For a given photon energy in the laboratory frame, the cross section will decrease if the photon emission angle is increased since $\omega_{\text{c.m.}}$ gets larger leaving less available phase space. We also observe that the rather pronounced angular distribution shown by the data in the high-energy region can be reproduced only for a relatively small value of the Fermi momentum as in the present case. In fact, the angular distribution becomes more and more isotropic as the Fermi momentum increases (see Fig. 4). This indicates that these energetic photons are originated more from the surface region rather than from the interior of the nucleus.

In Fig. 3 we show the results for $p + {}^{107}\text{Ag}$ with the same condition as in Fig. 2, but for very forward photon emission angle of $\theta = 30°$. Since in our model the dominant dependence on the target nucleus arises from the geometrical cross sectional area [see Eq. (2.9)] we have just rescaled the results for $p + \text{Tb}$ for $\theta = 30°$, i.e., the parameters of the model are the same as in Fig. 2. We see that the quality of the agreement with the data is similar to that of Fig. 2.

In the low-energy region ($\omega < 70$ MeV) our results underestimate the data by a factor of $\sim 2$. There are two ways to cure this problem within the present model. One way is to decrease the effective mass, as has been seen in Fig. 1, and at the same time also to decrease the value of the Fermi momentum $k_f$. The latter is necessary in order to keep the agreement with the data in the high-energy region. In fact, we can get a good agreement over the entire energy region if we choose $m^* \sim 0.7m$ and $k_f \sim 0.8$ fm$^{-1}$. However, this parameter set is not realistic because for such a low density we do not expect a small effective mass. The second possibility is that the low-energy photons come from a higher-density region than

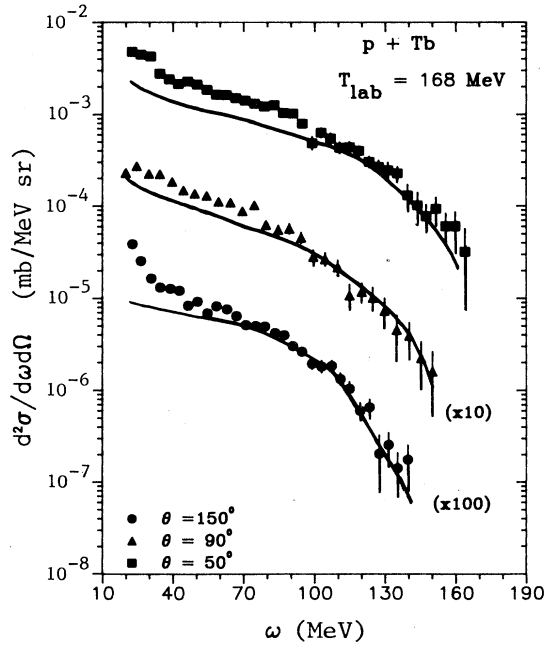


FIG. 2. The bremsstrahlung differential cross section (in the laboratory system) for $p + {}^{159}\text{Tb}$ at the incident energy of $T_{\text{lab}} = 168$ MeV as a function of photon energy and for different photon emission angle $\theta$. The values of the Fermi momentum and the effective mass are $k_f = 1.04$ fm$^{-1}$ and $m^* = 0.9m$, respectively. The data are from Ref. 8.

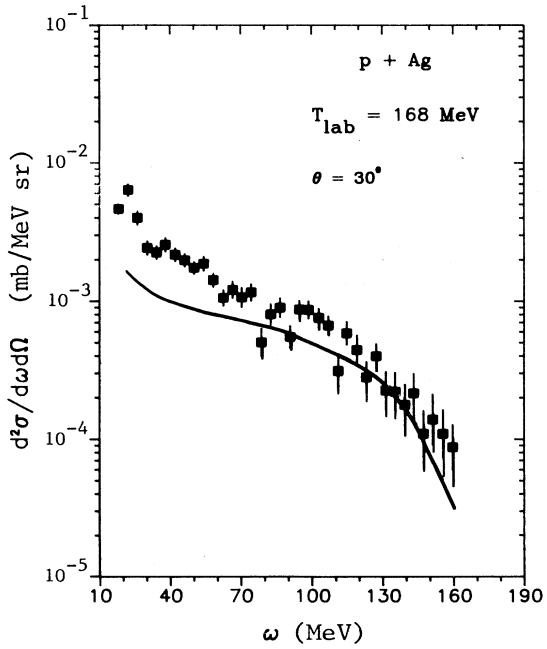


FIG. 3. The bremsstrahlung differential cross section (in the laboratory system) for $p + {}^{107}\text{Ag}$ at the incident energy of $T_{\text{lab}} = 168$ meV as a function of photon energy and for photon emission angle of $\theta = 30°$. The parameters are the same as in Fig. 2. The data are from Ref. 8.

the high-energy photons. For higher densities we have much stronger mean-field potential and consequently the cross section may increase. In order to illustrate this point, in Fig. 4 we show the results when we use $k_f = 1.36$ fm$^{-1}$ and $m^* = 0.7m$. Of course, we cannot answer the question here why low-energy photons would come from higher densities than high-energy photons. Perhaps some of the lower-energy photons come from multistep collision processes. Certainly, these are more important for low-energy photons than they are for high-energy photons.

We now examine the Fermi momentum dependence of the photon cross sections in more detail. The $k_f$ dependence enters in two ways:

(i) Neglecting the Pauli principle, the available phase space goes up when $k_f$ is increased. This is easily seen from Eq. (3.2); the average $p$ in this equation is larger when $k_f$ is increased.

(ii) Second, the Pauli blocking is more effective for forward photon emissions than for backward emissions. This can easily be visualized from Fig. 5, where the momenta of the nucleons before and after the photon emission are displayed together with the corresponding photon momentum. Around the target nucleon we have the Fermi sphere (actually an ellipsoid due to the Lorentz boost) which blocks the final-state phase space. Then, for high-energy photons, due to the recoil momentum $(-\mathbf{k}/2)$ of the scattered nucleons, it is easy to see that the Pauli blocking is more effective for forward photon emission than for backward emission.

From the above considerations it is clear that these two effects, (i) and (ii), of the Fermi momentum $k_f$ on the bremsstrahlung cross section work against each other.

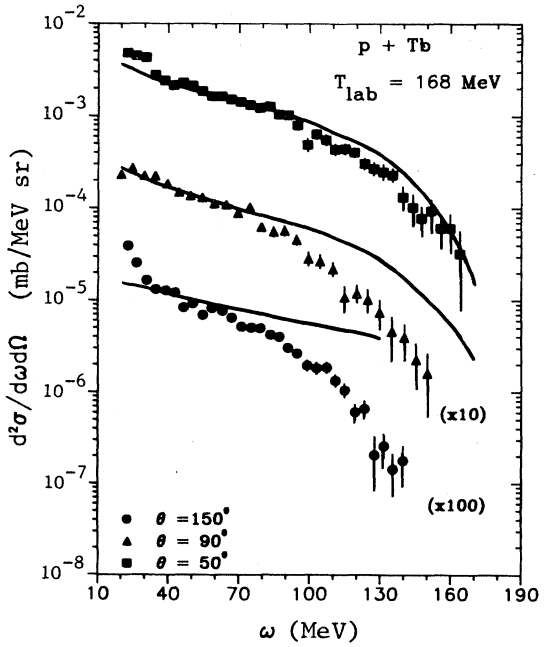


FIG. 4. Same as in Fig. 2, but for $k_f = 1.36$ fm$^{-1}$ and $m^* = 0.7m$.

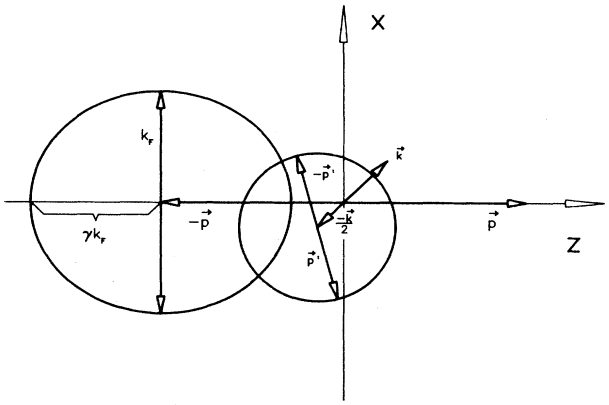


FIG. 5. The relative momenta of the two interacting nucleons in the initial nucleon-nucleon center-of-mass frame before ($\mathbf{p}$ and $-\mathbf{p}$) and after ($\mathbf{p}'$ and $-\mathbf{p}'$) the emission of a photon with momentum $\mathbf{k}$. The Lorentz boosted Fermi sphere with momentum $k_f$ blocks the final-state phase space around the target nucleon with momentum $-\mathbf{p}$. $\gamma$ is the usual Lorentz transformation parameter. The situation in the figure corresponds to the case where the target nucleon in the laboratory frame has its momentum along the $z$ direction.

The fact that the cross section is almost insensitive on $k_f$ for forward angles in the present case (compare Figs. 2 and 4, and also Figs. 6 and 7) is that they compensate each other. For backward emission angles the effect (i) dominates.

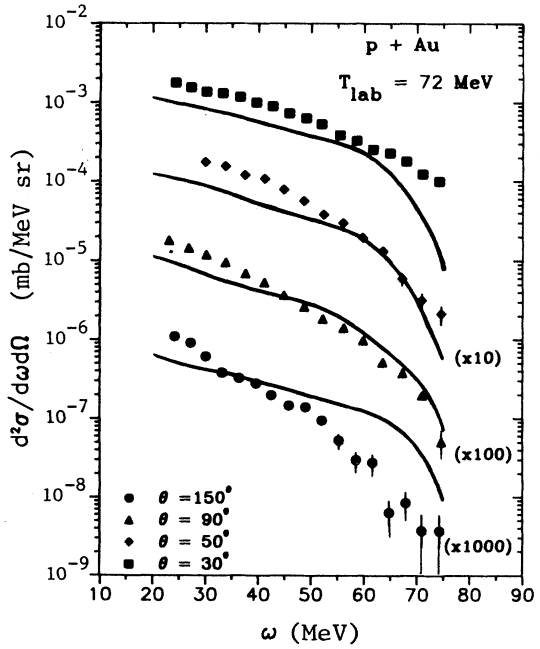


FIG. 6. The bremsstrahlung differential cross section (in the laboratory system) for $p + {}^{197}$Au at the incident energy of $T_{lab} = 72$ MeV as a function of photon energy and for various photon emission angle $\theta$. The values of the Fermi momentum and the effective mass are $k_f = 0.93$ fm$^{-1}$ and $m^* = 0.9m$, respectively. The data are from Ref. 7.

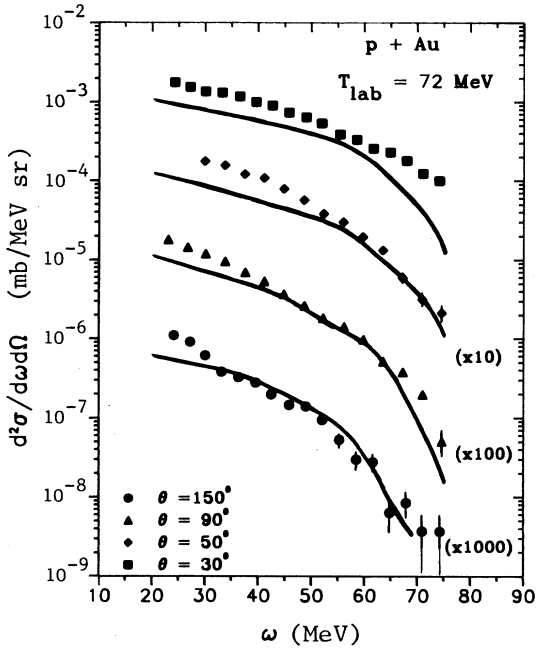


FIG. 7. Same as in Fig. 6, but for $k_f = 0.7$ fm$^{-1}$.

We next consider photon production at a lower incident energy, $p + {}^{197}$Au at $T_{lab} = 72$ MeV. Here we used a cross section of $\sigma \sim 86$ mb, which is a weighted average of the *pn* and *pp* cross sections at this energy. The interaction density is then $\sim \frac{1}{3}\rho_0$ and the equivalent Fermi momentum is 0.93 fm$^{-1}$. We have also chosen $m^* = 0.9m$ as in the previous case. We see from Fig. 6 that, although for $\theta = 50°$ and 90° the agreement seems reasonable, we cannot describe the data for very forward and backward angles. We might think that these high-energy photons come from a lower-density region than that corresponding to the value of $k_f$ estimated here. It may be that for these incident energies a simple estimate of the density as in Eq. (2.10) is not as good as for higher incident energies. To illustrate this, in Fig. 7 we show the results when the Fermi momentum is chosen to have the very small value of $k_f = 0.7$ fm$^{-1}$. The agreement now is much better for $\theta = 150°$. However, we still underestimate the data at $\theta = 30°$ which are a factor of $\sim 3-5$ larger than those at $\theta = 50°$. Such a strong angular dependence is not observed at higher incident energies (see Figs. 2 and 3). The reason for the strong sensitivity of high-energy photon cross sections on $k_f$ for backward photon emission angles has already been mentioned. A comparison of Figs. 6 and 7 reveals that, in the region of Fermi momentum involved here, the forward emission angle cross sections are insensitive to the value of $k_f$ even for high-energy photons. This means that the only way to increase the cross section at these angles is to decrease the effective mass while also decreasing the Fermi momentum at the same time in order to satisfy Eq. (2.14) (compare also Figs. 2 and 4). The point is that we will not be able to describe this strong angular dependence in the present model within a reasonable range of the Fermi momentum and the mean-field potential. We also mention that the elementary *pn* bremsstrahlung cross section does not show such a strong angular dependence,[14] although, this fact doesn't imply that the nucleon-nucleus bremsstrahlung cannot have a stronger angular dependence.

## IV. CONCLUSIONS

We have investigated the energetic photons produced in intermediate-energy nucleon-nucleus collisions considering the first chance *NN* collisional mechanism. The phase-space distribution of the target nucleus have been simulated by a Fermi sphere. For the elementary *NN* bremsstrahlung amplitude we use the parametrized version of Ref. 13 which reproduces the meson exchange potential model calculation of Ref. 6.

The present calculation reproduces rather well the recent data by the Grenoble group[8] at $T_{lab} = 168$ MeV and indicates that these hard photons are created in a rather low-density region in the nucleus ($\sim 40\%$ of the nuclear matter normal density). It also indicates that lower-energy photons are produced in a different way than the high-energy photons. It is very interesting to repeat the calculation within a model in which other processes, such as the contribution of secondary collisions, can be included. This will help a more complete understanding about the origin of low as well as high-energy photons.

The present model cannot describe the strong angular dependence shown by the data[7] at the incident energy of $T_{lab} = 72$ MeV. However, it is not clear whether the discrepancy is due to the inadequacy of our model. A more detailed calculation seems to be needed. On the other hand, it is of crucial importance to have more complete angular distribution data in order to clarify this problem.

*Note added in proof.* After submitting the present work for publication, we have learned from Pinston[17] that their data for $p + $Au at 72 MeV may contain a pile-up between photons and fast protons for forward photon emission angles ($\theta \sim 30°$). This could explain the disagreement between the present prediction and their data observed in the high-energy part of the $\gamma$ spectrum.

The authors wish to thank J. Pinston for providing us with his data prior to publication.

*Also at Department of Physics and Astronomy, University of Georgia, Athens, GA 30602.

[1]T. S. Biro, K. Niita, A. A. DePaoli, W. Bauer, W. Cassing, and U. Mosel, Nucl. Phys. **A475**, 579 (1987).
[2]B. A. Remington, M. Blann, and G. F. Bertsch, Phys. Rev. C **35**, 1720 (1987).
[3]R. Hingmann *et al.*, Phys. Rev. Lett. **58**, 759 (1987).
[4]V. Metag, Nucl. Phys. **A482**, 483c (1988).
[5]K. Kwato Njock, M. Maurel, E. Monnand, H. Nifenecker, J. A. Pinston, F. Schussler, D. Barneoud, and Y. Schutz, Nucl.

Phys. **A482**, 489c (1988).
[6]K. Nakayama, Phys. Rev. C **39**, 1475 (1989).
[7]K. Kwato Njock, M. Maurel, H. Nifenecker, J. A. Pinston, F. Schussler, D. Barneoud, S. Drissi, J. Kern, and J. P. Vorlet, Phys. Lett. B **207**, 269 (1988).
[8]J. A. Pinston, D. Barneoud, V. Bellini, S. Drissi, J. Guillot, J. Julien, M. Kwato Njock, M. Maurel, H. Nifenecker, F. Schussler, and J. P. Vorlet, Phys. Lett. B **218**, 128 (1989); J. A. Pinston, private communication.
[9]J. Edgington and B. Rose, Nucl. Phys. **89**, 523 (1966).
[10]K. Nakayama, S. Drozdz, S. Krewald, and J. Speth, Nucl. Phys. **A470**, 573 (1987); **A484**, 685 (1988).
[11]M. R. Anastasio, L. S. Celenza, W. S. Pong, and C. M. Shakin, Phys. Rep. **100**, 327 (1983).
[12]V. R. Brown and J. Franklin, Phys. Rev. C **8**, 1706 (1973).
[13]K. Nakayama and G. F. Bertsch, Phys. Rev. C **40**, 685 (1989).
[14]V. Herrmann, J. Speth, and K. Nakayama, Phys. Rev. C (submitted).
[15]H. W. L. Naus and J. H. Koch, Phys. Rev. C **39**, 1907 (1989); J. H. Koch, private communication.
[16]J. Franz, H. P. Grotz, L. Lehmann, E. Rossle, H. Schmitt, and L. Schmitt, Nucl. Phys. **A490**, 667 (1988).
[17]J. Pinston, private communication.